Assessing Hydrologic Impact of Climate Change with Uncertainty Estimates: Bayesian Neural Network Approach

MOHAMMAD SAJJAD KHAN

Ontario Ministry of the Environment, Sudbury, Ontario, Canada

PAULIN COULIBALY

Department of Civil Engineering and School of Geography and Earth Sciences, McMaster University, Ontario, Canada

(Manuscript received 9 February 2009, in final form 18 August 2009)

ABSTRACT

A major challenge in assessing the hydrologic effect of climate change remains the estimation of uncertainties associated with different sources, such as the global climate models, emission scenarios, downscaling methods, and hydrologic models. There is a demand for an efficient and easy-to-use rainfall–runoff modeling tool that can capture the different sources of uncertainties to generate future flow simulations that can be used for decision making. To manage the large range of uncertainties in the climate change impact study on water resources, a neural network–based rainfall–runoff model—namely, Bayesian neural network (BNN)—is proposed. The BNN model is used with Canadian Centre for Climate Modelling and Analysis Coupled GCM, versions 1 and 2 (CGCM1 and CGCM2, respectively) with two emission scenarios, Intergovernmental Panel on Climate Change (IPCC) IS92a and Special Report on Emissions Scenarios (SRES) B2. One widely used statistical downscaling model (SDSM) is used in the analysis. The study is undertaken to simulate daily river flow and daily reservoir inflow in the Serpent and the Chute-du-Diable watersheds, respectively, in northeastern Canada. It is found that the uncertainty bands of the mean ensemble flow (i.e., flow simulated using the mean of the ensemble members of downscaled meteorological variables) is able to mostly encompass all other flows simulated with various individual downscaled meteorological ensemble members whichever CGCM or emission scenario is used. In addition, the uncertainty bands are also able to typically encompass most of the flows simulated with another rainfall–runoff model, namely, Hydrologiska Byråns Vattenbalansavdelning (HBV). The study results suggest that the BNN model could be used as an effective hydrological modeling tool in assessing the hydrologic effect of climate change with uncertainty estimates in the form of confidence intervals. It could be a good alternative method where resources are not available to implement the general multimodel ensembles approach. The BNN approach makes the climate change impact study on water resources with uncertainty estimate relatively simple, cost effective, and time efficient.

1. Introduction

The estimation of future river flow regime at watershed scale, considering climate change impact, varies significantly with global climate models (GCliMs), greenhouse gas emission scenarios, downscaled meteorological ensembles, and rainfall–runoff models. Using one GCliMs with one greenhouse gas emission scenario, one downscaled ensemble member of meteorological variable, and one rainfall–runoff model will provide only one possible estimate of flow regime, which provides insufficient information for decision making. To account for the various sources of uncertainties, a multimodel ensembles approach is recommended (Fowler et al. 2007; Christensen et al. 2007). A range of flow series can be generated with a range of models and emission scenarios, making uncertainty management task enormous, costly, and time consuming. A simplified method is needed to overcome those practical limitations.

Uncertainty management in climate change impact study on water resources is becoming increasingly important, as water managers are beginning to use climate change projections in resource planning. Many impact studies did not consider the uncertainty of their water estimate, which, according to Hulme and Carter (1999), is a dangerous practice and should be avoided as much as

Corresponding author address: Mohammad S. Khan, 199 Larch St., Suite 1201, Sudbury ON P3E 5P9, Canada.
E-mail: sajjad_km@hotmail.com

DOI: 10.1175/2009JHM1160.1

possible (Prudhomme et al. 2003). To capture the range of uncertainties, McCarthy et al. (2001) recommends using many GCliMs, emission scenarios, and downscaled meteorological ensembles. This results in an implausible amount of work—which is not easily doable in many cases owing to time and resources limitation. Prudhomme et al. (2003) calculated uncertainty by estimating the confidence interval in flood quartiles using the bootstrap method for four different catchments in the United Kingdom. To represent a range of uncertainty in climate model outputs, Prudhomme et al. (2003) used Monte Carlo simulation for generating 25 000 climate scenarios, using several global climate models, emission scenarios, climate sensitivities, and excluding uncertainty because of downscaling techniques. Sometimes empirical relationships between hydrological and climate indicators and their standard errors are used for estimating uncertainties. For example, some hydrological indicators (such as the T-year flood) can be estimated from relatively simple climate indices by empirical relationships. Such relationships can give an indication of the standard error of estimation, and it is therefore possible to use such relationships with simple climate indicators to look at uncertainty in estimates of climate change impact. The empirical relationships may not be as ''good'' as model-based estimates, but the benefits of using them in terms of risk identification may outweigh the extra computational time needed by the models. There are some limitations of this empirical method, such as many hydrological indicators (such as reservoir reliability) cannot be estimated from such simple relationships (Arnell, 1999).

In the study by Wilby and Harris (2006), a probabilistic framework for assessing uncertainties in climate change impact on low flow is presented for the River Thames, United Kingdom. The probabilistic framework combined information from an ensemble of four general circulation models (GCMs), two greenhouse gas emission scenarios, two statistical downscaling techniques, two hydrological model structures, and two sets of hydrological model parameters. GCMs were weighted according to an index of reliability for downscaled effective rainfall, a key determinant of low flows in the River Thames. Hydrological model structures were weighted by performance at reproducing annual low-flow series. Weights were also assigned to sets of water resource model parameters using the Nash–Sutcliffe efficiency criterion. Emission scenarios and downscaling methods were unweighted. A Monte Carlo approach was then used to explore components of uncertainty affecting projections for the River Thames by the 2080s. Some studies rely on using multiple downscaling and hydrologic models (Dibike and Coulibaly 2005, 2007). More recently, Coulibaly (2008) used a multimodel approach focusing on uncertainties associated with different downscaling methods and different hydrologic models. It was shown that a major source of uncertainty in hydrologic impact study is associated with the downscaling method. It was also observed that although the multimodel approach appears appropriate for capturing the various sources of uncertainties, its implementation requires large human and computational resources, and it is still unclear how many models should be considered optimal.

Although there are various methods of uncertainty estimation, their integration into the climate change impact study on water resources is not straightforward. Therefore, the objective of this research is to introduce a simple method that can be used as an effective hydrological modeling tool to encompass uncertainties ranging from different GCliMs and emission scenarios, diverse ensemble members of downscaled meteorological variables, and another hydrological model.

The paper is organized as follows. In section 2, a brief description of the two Canadian GCMs is provided. In section 3, the downscaling method is presented, and in section 4, a description of the Bayesian neural network (BNN) model is provided. Section 5 discusses the sources of uncertainty and the BNN modeling approach. In sections 6 and 7, the results of climate change impact on river flow and reservoir inflow with uncertainty estimates using the BNN model are presented and discussed. In section 8, a summary and conclusions about the study are drawn.

2. Global climate model

A GCliM is a large-scale numerical model that simulates the physical processes that affect the climate. They solve three-dimensional calculations of the physical equations that describe the complex interactions among the atmosphere, ocean, cryosphere, and land surface. GCliMs relate changes in atmospheric chemistry to changes in climate variables, such as temperature, precipitation, wind, clouds, radiation, and snow cover (Frederic and Major 1997). The two versions of the Canadian Centre for Climate Modelling and Analysis Coupled GCMs [CGCMs, version 1 and 2 (CGCM1 and CGCM2)] and two greenhouse gas emission scenarios were used in the current research. CGCM1 and its control climate are described by Flato et al. (2000). The atmospheric component of the model has a surface grid resolution of roughly $3.7° \times 3.7°$ and 10 vertical levels, which is described in detailed by McFarlane et al. (1992). The ocean component is based on the U.S. Geophysical Fluid Dynamics Laboratory (GFDL) Modular Ocean Model (MOM) and has a resolution of roughly $1.8° \times 1.8°$ and 29 vertical levels.

CGCM2 is the improved version of the CGCM1, addressing a few shortcomings identified in the first version. In particular, the ocean mixing parameterization has been changed from the horizontal/vertical diffusion scheme to the isopycnal–eddy stirring parameterization of Gent and McWilliams (1990), and sea ice dynamics has been included following Flato and Hibler (1992). A description of CGCM2 and a comparison to CGCM1 with regard to its response to increasing greenhouse gas forcing can be found in Flato and Boer (2001).

The emission scenario considered is the Intergovernmental Panel on Climate Change (IPCC) IS92a forcing scenario, in which the change in greenhouse gases forcing corresponds to that observed from 1900 to 1990 and increases at a rate 1% per year thereafter until year 2100. The direct effect of sulfate aerosols is also included. This scenario is often considered as the ''business as usual scenario.'' The second greenhouse gas forcing scenario considered is IPCC Special Report on Emissions Scenarios (SRES) B2, in which simulations begin at year 1990 with initial conditions from the corresponding member of IS92a runs. The B2 scenario considers slower population growth (10.4 billion people by 2100) with a more rapidly evolving economy and more emphasis on environmental protection. It is therefore a conservative scenario that produces lower emissions and less future warming.

3. Downscaling model

A statistical downscaling model (SDSM; Wilby et al. 2002) is used to derive local-scale meteorological data (daily precipitation and temperature) from the CGCM-simulated large-scale climate indicators. Because of its relative competitiveness, robustness, and lower cost, the statistical downscaling model is chosen over a dynamical downscaling technique. An overview of statistical and dynamical downscaling techniques can be found in Coulibaly et al. (2005), and a comprehensive review of downscaling methods is provided by Fowler et al. (2007).

A SDSM is a multiple regression method that is currently one of the most largely used methods for generating high-resolution ensembles of meteorological data from GCM outputs. Suitability of this model was verified by comparing its performance with other two commonly used statistical downscaling models: a nonlinear regression based on a temporal neural network (TNN) model (Coulibaly et al. 2005) and a stochastic method based on the Long Ashton Research Station weather generator (LARS-WG) model (Semenov and Barrow 1997). The comparative study of these three statistical downscaling models was undertaken separately, using the observed large-scale National Centers for Environmental Prediction (NCEP) reanalysis climate predictors and the CGCM-simulated climate predictors for the period of 1961–2000 (Khan et al. 2006a,b). Various statistics of observed and downscaled daily maximum and minimum temperature and daily precipitation were compared. In daily maximum and minimum temperature downscaling, analyses were undertaken by comparing monthly mean and variances at the 95% confidence level between observed and downscaled data. In addition, uncertainty (calculated by 95% confidence intervals) of the monthly means and variances of downscaled and observed daily maximum and minimum temperatures was compared. In daily precipitation downscaling, in addition to comparing means and variances, monthly-mean dry and wet spell lengths and their 95% confidence intervals, cumulative frequency distributions (cdfs) of the monthly mean of daily precipitation and the distributions of monthly wet and dry days for observed and downscaled daily precipitation were compared. A detailed comparison of various statistics in the two separate studies showed that the SDSM is the most skilled model for reproducing the observed statistics in its downscaled data as opposed to the TNN and LARS-WG models. Because of this robustness, the SDSM has been considered as an appropriate downscaling model for this study. In the current research, the SDSM is calibrated and validated using observed large-scale NCEP reanalysis predictors and local-scale predictands (daily precipitation and temperature) for the watersheds under study.

4. Bayesian neural network

The BNN is used as a hydrologic model to simulate flow corresponding to various ensemble members of downscaled precipitation and temperature under climate change scenarios. Appropriateness of the BNN model in rainfall–runoff modeling was investigated for the same watershed by Khan and Coulibaly (2006). Its performance was found competitive with a widely used integrated hydrologic modeling system (IHMS)—namely, the Hydrologiska Byråns Vattenbalansavdelning (HBV)—developed at the Swedish Meteorological and Hydrological Institute (SMHI 1996). The performance of the BNN was also found to be superior to the most commonly used neural network model, the multilayer perceptron (MLP). The inherent advantage of the BNN model is its uncertainty estimation capacity of simulated flow in the form of confidence intervals. This uncertainty estimation capacity of the BNN model is exploited in the current research to investigate its effectiveness for capturing uncertainties cascaded into downscaled ensemble members of daily precipitation and temperature sourced from two versions of CGCM and two emission scenarios. The

description of the BNN model is limited in this paper; for a more detailed description, refer to Khan and Coulibaly (2006) and Nabney (2004).

In the Bayesian learning approach, the method starts with a suitable prior distribution, $p(\mathbf{w})$ for the network parameters (weights and biases). Once the data D is observed, Bayes's theorem is used for writing an expression of the posterior probability distribution for the weights $p(\mathbf{w}|D)$ as follows:

$$p(\mathbf{w}|D) = \frac{p(D|\mathbf{w})p(\mathbf{w})}{p(D)}, \tag{1}$$

where $p(D|\mathbf{w})$ is the dataset likelihood function and the denominator $p(D)$ is a normalization factor, which can be obtained by integrating over the weight space as follows:

$$p(D) = \int p(D|\mathbf{w})p(\mathbf{w})\, d\mathbf{w}. \tag{2}$$

This ensures that the left-hand side of (1) gives unity when integrated over all the weight space. Once the posterior has been calculated, every type of inference is made by integrating over that distribution. Therefore, in implementing the Bayesian method, expressions for $p(\mathbf{w})$ and $p(D|\mathbf{w})$ are needed. The prior distribution, $p(\mathbf{w})$, which is not related to data, can be expressed in terms of weight-decay regularizer $E_W = \frac{1}{2}\sum_{i=1}^{W} w_i^2$, where W is the total number of weights and biases in the network. Similarly, the likelihood function in Bayes's theorem (1), which is dependent on data, can be expressed in terms of error function $E_D = (\frac{1}{2})\sum_{n=1}^{N}[y^n(\mathbf{x}^n; \mathbf{w}) - t^n]^2$, where $\mathbf{x}$ is the input vector, t is the target value, and $y(\mathbf{x}; \mathbf{w})$ is the network output. Upon deriving the expressions for the prior and likelihood functions, and using those expressions in (1), the posterior distribution of weights can be obtained. The objective function in the Bayesian method corresponds to the inference of the posterior distribution of the network parameters. After defining the posterior distribution (objective function), the network is trained with a suitable optimization algorithm to maximize the posterior distribution $p(\mathbf{w}|D)$. Thus, the most probable value for the weight vector $\mathbf{w}_{\mathrm{MP}}$ corresponds to the maximum of the posterior probability. Using the rules of conditional probability, the distribution of outputs, for a given input vector $\mathbf{x}$ can be written in the form

$$p(t|\mathbf{x}, D) = \int p(t|\mathbf{x}, \mathbf{w})p(\mathbf{w}|D)\, d\mathbf{w}, \tag{3}$$

where $p(t|\mathbf{x}, \mathbf{w})$ is simply the model for the distribution of noise on the target data for a fixed value of the weight vector $\mathbf{w}_{\mathrm{MP}}$, and $p(\mathbf{w}|D)$ is the posterior distribution of the weights.

To make the integration analytically tractable and also if the dataset is large, $p(\mathbf{w}|D)$ may be approximated to a Gaussian distribution (Walker 1969; MacKay 1992a,b; Nabney 2004). After some simplification, the integral in (3) can be written after Bishop (1995) as

$$p(t|\mathbf{x}, D) = \frac{1}{(2\pi\sigma_t^2)^{1/2}} \exp\left\{-\frac{[(t-y)(\mathbf{x}; \mathbf{w}_{\mathrm{MP}})]^2}{2\sigma_t^2}\right\}. \tag{4}$$

This distribution has a mean given by $y(\mathbf{x}; \mathbf{w}_{\mathrm{MP}})$ and a variance given by

$$\sigma_t^2 = \frac{1}{\beta} + \mathbf{g}^{\mathrm{T}}\mathbf{A}^{-1}\mathbf{g}, \tag{5}$$

where β is a hyperparameter, which is actually the inverse variance of the noise model; $\mathbf{g}$ denotes the gradient of $y(\mathbf{x}, \mathbf{w})$ with respect to the weights $\mathbf{w}$ evaluated at $\mathbf{w}_{\mathrm{MP}}$; and $\mathbf{A}$ is the Hessian matrix of the total (regularized) error function, with elements given by

$$\mathbf{A} = \nabla\nabla S(\mathbf{w}_{\mathrm{MP}}) = \beta\nabla\nabla E_D(\mathbf{w}_{\mathrm{MP}}) + \alpha\mathbf{I}, \tag{6}$$

where $\mathbf{I}$ is the identity matrix. The standard deviation σ_t of the predictive distribution for the target t can be interpreted as an error bar on the mean value $y(\mathbf{x}; \mathbf{w}_{\mathrm{MP}})$.

The major challenge in the Bayesian approach is evaluating integrals for the posterior distribution of weights as well as the predictive distribution of network outputs. Those integrals are analytically tractable for a small class of prior and likelihood functions. The dimensionality of the integrals is given by the number of network parameters, so simple numerical algorithms do not work in this case. This is why the use of approximations to the posterior, such as Gaussian, or numerical methods for evaluating integrals, such as Monte Carlo methods combined with Markov chain (MCMC) sampling, play such a large role in the use of Bayesian methods with neural networks. Gaussian approximation was described earlier, and the Monte Carlo method is described briefly later in this paper, which has been developed by Neal (1992, 1993, 1996). In that so-called full Bayesian approach, the integral in (3) is approximated by finite sums of the form

$$p(t|\mathbf{x}, D) \approx \frac{1}{N}\sum_{n=1}^{N} p(t|\mathbf{x}, \mathbf{w}_n), \tag{7}$$

where $\mathbf{w}_n$ represents a MCMC sample of weight vectors generated from the distribution $p(\mathbf{w}|D)$. The implementation of MCMC approximation for complex real-world problems remains a challenging task because of

the problem of convergence and the computational cost. Although the MCMC method has been successfully used in some applications (Lampinen and Vehtari 2001; Kingston et al. 2005; Jana et al. 2008), the problem of convergence and computational complexity remains an issue for practical applications and thus explains why it is not widely adopted by practical users. Furthermore, there is no well-established method for selecting which approximation method to use for a given a problem. The choice of approximation method is typically problem dependent (Lampinen and Vehtari 2001). Therefore, given the complexity and the large datasets involved in the hydrologic impact simulation, Gaussian approximation is preferred because it has been shown to perform well for rainfall–runoff modeling in the same study area. Other reasons why the posterior distribution has been approximated to Gaussian include the good length of data available for network training and analytical simplicity.

The BNN modeling is implemented in this work using a MLP network. The network architecture includes one hidden layer with tangent hyperbolic (tanh) activation function and one output layer with a linear processing unit. The common trial-and-error approach has been used in network training with stopping criterion, such as root-mean-square error (RMSE), Nash–Sutcliffe efficiency index R^2, and correlation coefficient r. The optimum number of processing units for river flow prediction using BNN was 20 and for reservoir inflow simulation, it was 10.

The initial values of the weights and biases are obtained from a Gaussian prior distribution of zero mean and inverse variance α (also known as regularization coefficient or prior hyperparameter). The Gaussian prior has been chosen to favor small values for the network weights because a network with large weights will usually give rise to a mapping with large curvature (Nabney 2004). Moreover, the Gaussian prior also provides computational simplicity. For α, a single initial value has been chosen for both hidden and output layer weights. It is assumed that the target data are generated from a smooth function with additive zero-mean Gaussian noise. Thus, for the noise model, a Gaussian distribution with zero mean and constant inverse variance β is used. For hyperparameter β, a single initial value has been chosen for both the hidden and output layer weights. The network training is completed by the trial-and-error approach, as mentioned earlier, and the network weights are optimized using the "scaled conjugate gradients" optimization technique to find the most probable weights $\mathbf{w}_{\mathrm{MP}}$ by maximizing the posterior distribution of weights $p(\mathbf{w}|D)$, or it can be said by minimizing the error function $S(\mathbf{w})$. The hyperparameters α and β have also been optimized during the training process using the evidence procedure (Bishop 1995) in which the hyperparameters are set to values that maximize the evidence of the model $p(D|\alpha, \beta)$.

TABLE 1. BNN model performance statistics of validation results.

	River flow	Reservoir inflow
RMSE ($m^3\ s^{-1}$)	6.45	46.69
R^2	0.97	0.95
r	0.99	0.98
PFC	0.09	0.11
LFC	0.14	0.32

Once the network has been trained, the predictions are completed using (4) in which posterior distribution has been approximated to Gaussian. The posterior distribution has been approximated to Gaussian because of the good length of data available, and also because of analytical simplicity. The error bars for the predictions have been calculated using (5). The 95% confidence intervals of the mean network output $y(\mathbf{x}; \mathbf{w}_{\mathrm{MP}})$ have been estimated by adding and subtracting 2σ from $y(\mathbf{x}; \mathbf{w}_{\mathrm{MP}})$. This experiment has been conducted using MATLAB routines provided by Nabney (2004).

Model validation statistics such as RMSE, R^2, r, peak flow criteria (PFC), and low-flow criteria (LFC) for river and reservoir inflow simulation are presented in Table 1. The RMSE statistic provides a general illustration of the overall accuracy of the predictions, as it shows the global goodness of the fit by incorporating the random errors and biases in its calculation. A low value of RMSE indicates a good model fit to the data. The R^2 statistic explains variance around the mean. The value of R^2 ranges from $-\alpha$ for the worst case to $+1$ for a perfect fit. According to Shamseldin (1997), an R^2 of 0.9 or more indicates a very satisfactory model, 0.8–0.9 represents a fairly good model, and less than 0.8 is deemed unsatisfactory. The correlation coefficient r measures the variance of observed flow that is explained by the model; r ranges from -1 (perfect negative correlation) through 0 (no correlation) to $+1$ (perfect positive correlation). PFC and LFC have been used to evaluate the model performance for peak flow and low-flow prediction. The criteria are described in a work by Coulibaly et al. (2001a). The PFC and LFC provide more accurate measures of the model performance than the RMSE for extreme value prediction. A PFC or LFC equal to 0 represents a perfect fit.

The discussion is focused only on the validation results because they provide factual evaluation information about the model performance as a result of the use of independent datasets from calibration. The model validation statistics provided in Table 1 are quite satisfactory. For example, the RMSE for the river flow is

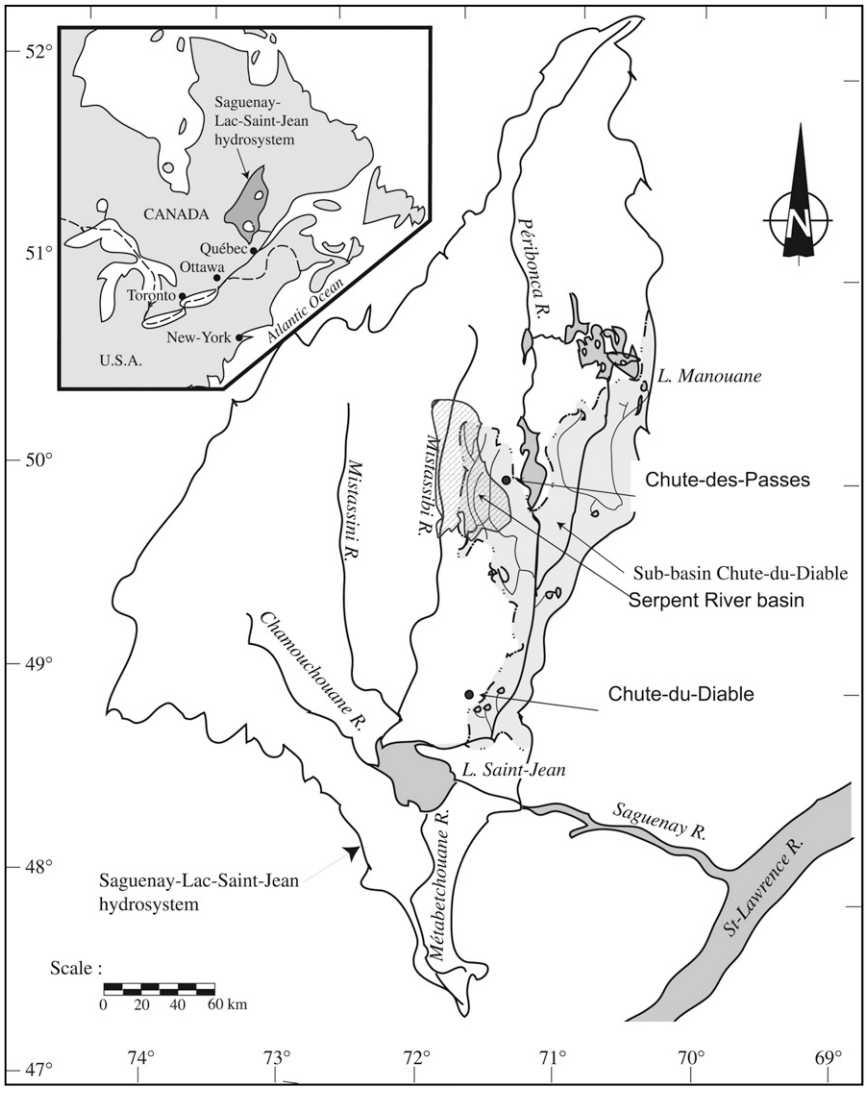

FIG. 1. Location map of the Serpent River subbasin and the CDD subbasin within the SLSJ watershed (Coulibaly et al. 2001b).

6.45 and 46.69 $m^3\ s^{-1}$ for the reservoir inflow. The R^2 value for the river flow is 0.97 and 0.98 for the reservoir inflow. The r value for the river flow is 0.99 and 0.98 for the reservoir inflow. The PFC statistic for the river flow is 0.09 and 0.11 for the reservoir inflow. The LFC for the river flow is 0.14 and 0.32 for the reservoir inflow. All those statistics are quite satisfactory and indicate that the BNN model is effective at simulating the river flow and the reservoir inflow. Therefore, the model can be applied for hydrologic impact simulation under climate change scenarios.

5. Sources of uncertainty and BNN modeling

In this hydrologic impact study, the sources of uncertainty include (a) CGCM1 and CGCM2, (b) the two greenhouse gas emission scenarios, (c) the SDSM, and (d) the two rainfall–runoff models (BNN and HBV). The SDSM model has an inherent stochastic component that allows the generation of 100 ensemble members for each downscaled variable (e.g., daily precipitation, temperature). Those ensemble members represent the structural uncertainty of the downscaling model. Therefore, to account for the downscaling model uncertainty, different ensemble members (for example the 50th ensemble member, the 100th ensemble member, etc) as well as the mean of the 100 ensemble members are used. To manage the range of uncertainties due to the GCliMs, the greenhouse gas emission scenarios, the downscaling models, and the hydrologic models, we assume that the confidence limits of BNN predictions will bound all flow

TABLE 2. Selected large-scale predictor variables corresponding to each of the predictands during SDSM downscaling. All predictors, with the exception of wind direction, have been normalized with respect to the 1961–90 mean and standard deviation (SD).

Predictor variable	Description	Precipitation		Max temperature		Min temperature	
		CDD	CDP	CDD	CDP	CDD	CDP
Temp	Mean temperature	x	x	x	x	x	x
Mslp	Mean sea level pressure						
p__u	Zonal velocity component near surface						
p5_u	Zonal velocity component at 500-hPa height						
p8_u	Zonal velocity component at 850-hPa height						
p__v	Meridional velocity component near surface	x	x	x	x	x	
p8_v	Meridional velocity component at 850-hPa height	x	x				
p__z	Vorticity					x	x
p_zh	Divergence near surface						
p5zh	Divergence at 500-hPa height						
p8zh	Divergence at 850-hPa height	x	x				
p500	500-hPa geopotential height			x	x	x	x
p850	850-hPa geopotential height						x
s500	Specific humidity at 500-hPa height	x	x	x	x		x
s850	Specific humidity at 850-hPa height			x	x	x	x
Shum	Near-surface specific humidity			x	x	x	x

simulations using any combination of GCliMs, emission scenarios, downscaled ensemble members, and hydrologic model.

To assess this assumption, the mean of the 100 ensemble members is calculated for one CGCM and one greenhouse gas emission scenario. The mean for each predictor (precipitation, temperature) is then fed into the BNN model to generate flow series (or predicted flow) with confidence limits. The flow predictions using the mean of the 100 ensemble members are called *mean ensemble flow*. Subsequently, other flow predictions are produced using any random combination of GCliMs, emission scenarios, and downscaled ensemble members. Those various flow predictions are plotted with the first predictions (namely, mean ensemble flow) to see whether all the predictions are within the uncertainty bands of the mean ensemble flow. It is also verified whether the same uncertainty bands can contain flow simulated using another conceptual rainfall–runoff model, namely, HBV. If one uncertainty band can contain all possible flows from the different combinations, then there is no need to spend time running repetitive simulations for each of the 100 ensemble members along with combination of GCliMs and emission scenarios. The capacity of the BNN model for uncertainty estimation in this respect has been evaluated for river flow and reservoir inflow, and the results are discussed in sections 6 and 7, respectively.

6. Climate change impact on river flow

Climate change impact on river flow using the BNN model is studied on the Serpent River basin located in the Saguenay-Lac-Saint-Jean (SLSJ) hydrologic system in northern Quebec, Canada (Fig. 1). The area of the Serpent basin is 1760 km^2, characterized by forest cover and cold climate, with 30% of total precipitation accounting for snowfall occurring between the months of November and March. Previous studies in the region by Coulibaly et al. (2000) showed that the snowmelt runoff is responsible for high flows in the spring season, accounting for up to 40% of the annual flow volume. The mean daily temperature in the area ranges between −40° and +30°C. There are many reservoirs and dams in the Saguenay watershed, built primarily for hydropower production. The study area and data description follow that of Khan and Coulibaly (2006), and Khan et al. (2006a,b).

Basin-scale-observed meteorological data—such as daily precipitation, daily maximum and minimum temperatures—are obtained from the Chute-des-Passes (CDP) meteorological station (station ID 7061541) located near the Serpent River basin (Fig. 1) at 49.90°N, 71.25°W. Daily river flow is obtained from a hydrometric station (station ID 062214) located at 49.41°N, 71.22°W (Fig. 1). The network of hydrometric stations is being maintained by the Aluminum Company of Canada (Alcan) for hydropower generation and management. For 12 years (1991–2002), hydrometeorological data were used for the calibration (1991–1998) and validation (1999–2002) of the rainfall–runoff model. SDSM is used to downscale meteorological variables (daily precipitation, and daily maximum and minimum temperatures) for the period of 1961–2100 for the Chute-des-Passes station. Canadian climate models CGCM1 and CGCM2 along with two emission scenarios IPCC IS92a and B2, respectively, were considered. The computational grid for the climate model encompassing the study area is located

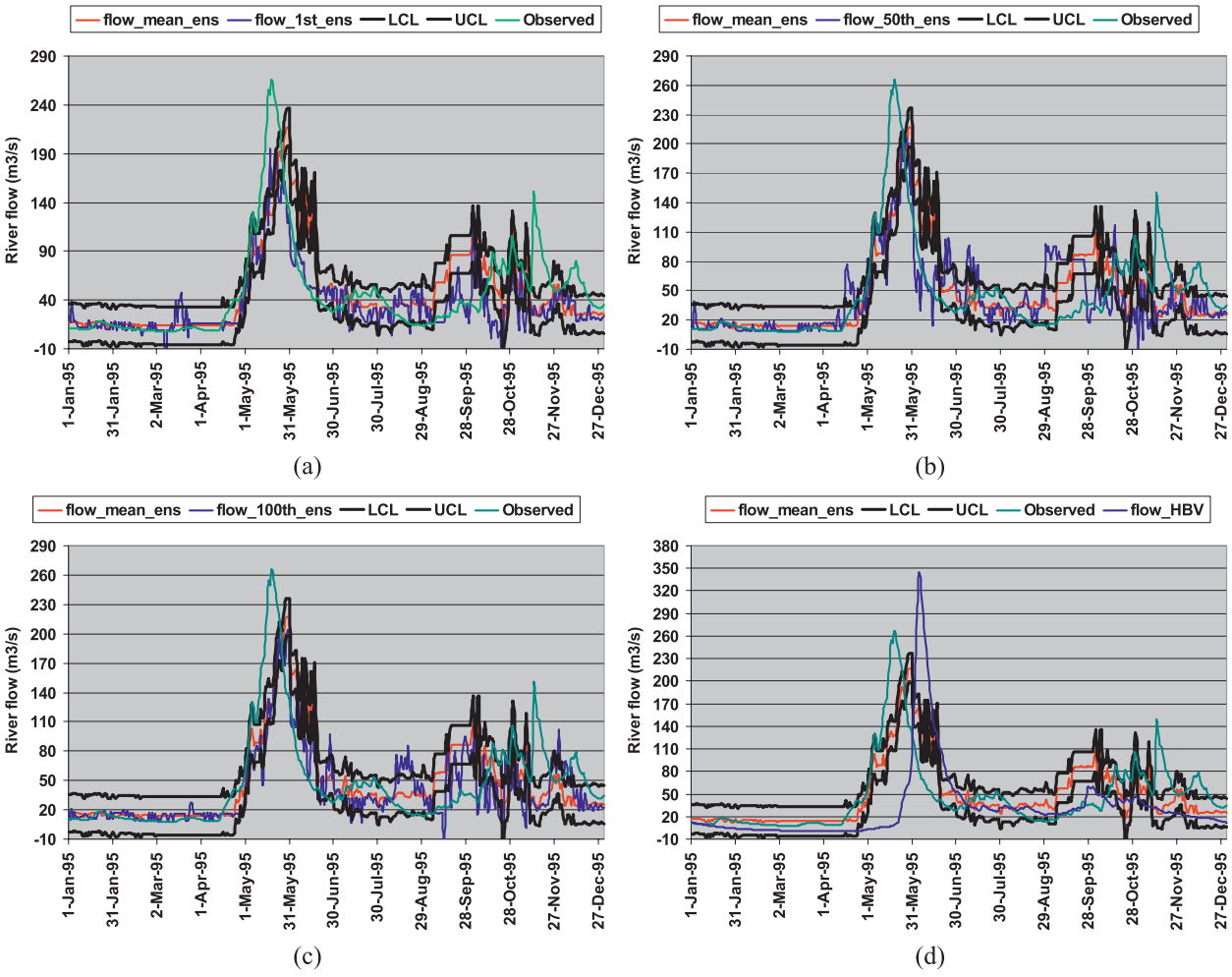

FIG. 2. Simulated river flow considering climate change impact for the year 1995. Observed flow, mean ensemble flow, and its upper and lower confidence limits are plotted in (a) 1st ensemble flow, (b) 50th ensemble flow, (c) 100th ensemble flow, and (d) HBV simulated flow.

at 50.10°N, 71.25°W. Selected large-scale atmospheric variables for downscaling daily precipitation, and daily maximum, and minimum temperatures are presented in Table 2.

The downscaled meteorological time series consists of 100 ensemble members of daily precipitation, and daily maximum and minimum temperatures, which were fed into the BNN model to simulate river flow. The optimum input combination for the BNN model for river flow simulation was the (i) total daily precipitation from the past seven days, starting from $t - 1$ to $t - 7$, was considered as seven separate inputs; (ii) moving sum of four weeks' snow as another input; (iii) mean daily temperature at $t - 1$; (iv) moving average of the last two weeks' mean daily temperature; and (v) months (January–December) as logical inputs to account for the seasonal variability. The selection of these predictor variables is based on a previous study on the same basin (Khan and Coulibaly 2006). The key objective of the current research is to assess if the uncertainty estimates (or uncertainty bands) of simulated flow using the mean of the 100 ensemble members of each downscaled meteorological variables (precipitation, temperature) with one version of CGCM forcing with one emission scenario are capable of encompassing all other simulated flows generated using any random combination of GCliMs, emission scenarios, and downscaled ensemble members. It is also our objective to prove that the uncertainty bands of the mean ensemble flow, which are generated using one version of CGCM with one emission scenario, are further capable of encompassing flows simulated with another version of CGCM with another emission scenario and also the flows simulated with another rainfall–runoff model. In the following discussion, the term *mean ensemble*

TABLE 3. Comparison of statistical properties for observed and simulated river flows (1995). The simulated river flow represents flow simulated by the BNN model using mean ensemble member of downscaled precipitation and temperature as inputs.

	Observed		Simulated	
	Mean ($m^3 s^{-1}$)	SD ($m^3 s^{-1}$)	Mean ($m^3 s^{-1}$)	SD ($m^3 s^{-1}$)
Jan	12.926	3.063	15.615	1.763
Feb	10.279	1.431	14.429	1.084
Mar	9.461	1.686	13.903	0.122
Apr	22.183	14.442	18.264	8.420
May	168.516	60.868	131.201	51.815
Jun	54.440	25.515	102.647	44.637
Jul	42.658	6.809	36.973	5.985
Aug	23.461	9.629	34.414	3.029
Sep	25.777	7.688	65.955	21.325
Oct	61.581	22.750	69.516	26.276
Nov	76.507	27.378	45.454	16.375
Dec	50.832	14.753	28.118	5.512

flow is used to describe the simulated flows using the mean of the 100 ensemble members of each downscaled meteorological variables (precipitation, temperature) fed into the BNN model. Similarly, the term *mean ensemble member* refers to the average of the 100 downscaled members of daily precipitation, and daily maximum and minimum temperatures, The terms *1st ensemble flow*, *50th ensemble flow*, *70th ensemble flow*, and *100th ensemble flow* are used to describe flows corresponding to the 1st, 50th, 70th, and 100th downscaled ensemble members, respectively. Recall that the SDSM, because of its stochastic component, generates 100 ensemble members (time series) for each of the downscaled variables (e.g., precipitation, temperature). Therefore, 1st ensemble member means the first member (or first series) of the 100 members. Similarly, the 50th ensemble member is the 50th member (or series) of the 100 members and so on. Flow series generated by feeding those ensemble members into the BNN model are called *ensemble flows*. For instance, when the 1st ensemble member is fed into the BNN model, the corresponding flow is named 1st ensemble flow; when the 2nd ensemble member is fed into the BNN model, the corresponding flow is named 2nd ensemble flow; and so on.

The results of the simulated flow along with the uncertainty bands are presented in Fig. 2 for the year 1995. In that figure, the mean flow and its 95% uncertainty bands are simulated using CGCM1 with IS92a emission scenario. For the clarity of presentation, only one year of data is presented. Observed daily flow for the year 1995 is also presented for comparison with the simulated flow. A comparison of basic statistics, such as mean and standard deviation for observed and simulated flow, for the same year is also presented in Table 3. The statistics in some months, especially the standard deviations, are quite different between the observed and simulated flow; however, the 95% uncertainty bands of the simulated flow mostly include the observed flow with some exception for the spring peak flow periods. For further comparison, the simulated flow for the 1st ensemble member of downscaled meteorological variables for CGCM1 IS92a emission scenario is plotted in Fig. 2a. The uncertainty bands of the mean ensemble flow mostly encompass both the observed and simulated flows with the 1st ensemble member. In Figs. 2b and 2c, the 50th and 100th ensemble flows were plotted, which were derived using CGCM2 SRES B2, whereas the mean ensemble flow and its confidence intervals were generated using CGCM1 IS92a emission scenario. This shows that the confidence intervals of the mean ensemble flow obtained with one CGCM forced with one emission scenario can almost entirely encompass other ensemble flows generated using another CGCM forced with another emission scenario. Figure 2d represents flow simulated with another hydrological model, HBV, with CGCM1 and IS92a emission scenario, referred to as ''flow_HBV'' in Fig. 2d, where the mean ensemble flow and its confidence intervals are derived from the same CGCM and emission scenario. The confidence intervals in this case encompassed the HBV-simulated flow most of the time during the year, except during the peak flow period around the month of May. Note that during that month, HBV-simulated flow is also not very close to the observed flow, indicating that there could be some limitations associated with the HBV model itself. This highlights the critical issue of model error in the hydrologic impact study. Note that HBV is a conceptual hydrological model in which various complex physical processes of the watershed have been simplified using mathematical equations and parameters. This simplification of the very complex nonlinear rainfall–runoff relationship could be a source of model error.

Simulated flow with climate change impact for the year 2037 is presented in Fig. 3. The mean ensemble flow and its 95% confidence intervals in Figs. 3a–3d are simulated using CGCM1 IS92a emission scenario. In Fig. 3a, the 1st ensemble flow is simulated using CGCM1 IS92a emission scenario; in Figs. 3b and 3c, the 70th and 100th ensemble flows were simulated using CGCM2 SRES B2. In Fig. 3d, the HBV-simulated flow is obtained with CGCM1 IS92a emission scenario. In all the cases, the confidence intervals of the mean ensemble flow of one CGCM with one emission scenario almost entirely encompasses all other simulated flows with another CGCM and emission scenario as well as with another hydrological model. This suggests that, in dealing with uncertainty with regard to hydrologic impact of climate change, there

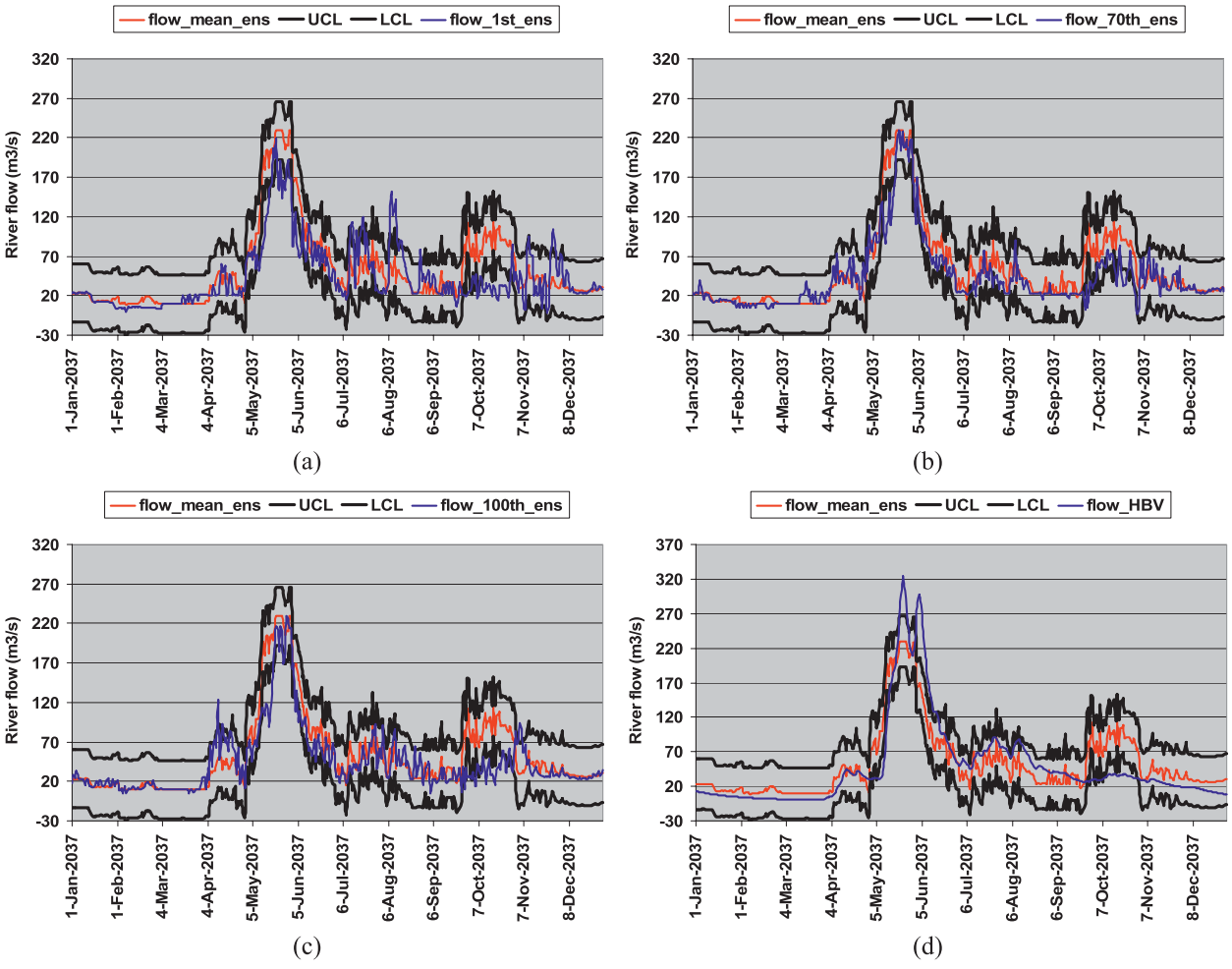

FIG. 3. As in Fig. 2, but for 2037.

is explicitly no need to use various individual downscaled members, rather it would be enough to use the mean ensemble flow and its uncertainty bands to represent the range of uncertainties associated with the two versions of CGCM and with the two emission scenarios, and with the hydrological model. This hypothesis is further proved in reservoir inflow simulation considering climate change impact on another watershed, which is described in the following section.

7. Climate change impact on reservoir inflow

Climate change impact on reservoir inflow is investigated on the Chute-du-Diable (CDD) subbasin (Fig. 1). The area of the watershed is 9700 km^2 and has reliable hydrometeorological data dating back to 1952. The entire Chute-du-Diable watershed contributes to the reservoir inflow. The data used in the study were total daily precipitation in the form of liquid and snow, daily maximum and minimum temperatures, and mean daily reservoir inflow. Daily precipitation and temperature data were obtained from the CDP and CDD meteorological stations, station ID numbers 7061541 and 7061560, respectively. The coordinates of the stations CDP and CDD were 49.9°N, 71.25°W and 48.75°N, 71.7°W, respectively (Fig. 1). A total of 40 years (1961–2000) of hydrometeorological data were used in the calibration (1961–90, 30 years) and validation (1991–2000, 10 years) of the downscaling of hydrologic models. The downscaling model is calibrated and validated using observed large-scale NCEP climate predictors and local-scale meteorological predictands of daily precipitation and daily maximum and minimum temperatures of the stations CDP and CDD for the period of 1961–2000. Selected large-scale GCM predictors for the two meteorological stations are presented in Table 2. The description of the study area and data used follow Khan and Coulibaly (2006) and Khan et al. (2006a,b). The calibrated downscaling model is used to downscale daily precipitation and temperature for the CDD and CDP stations, starting from 1961 to

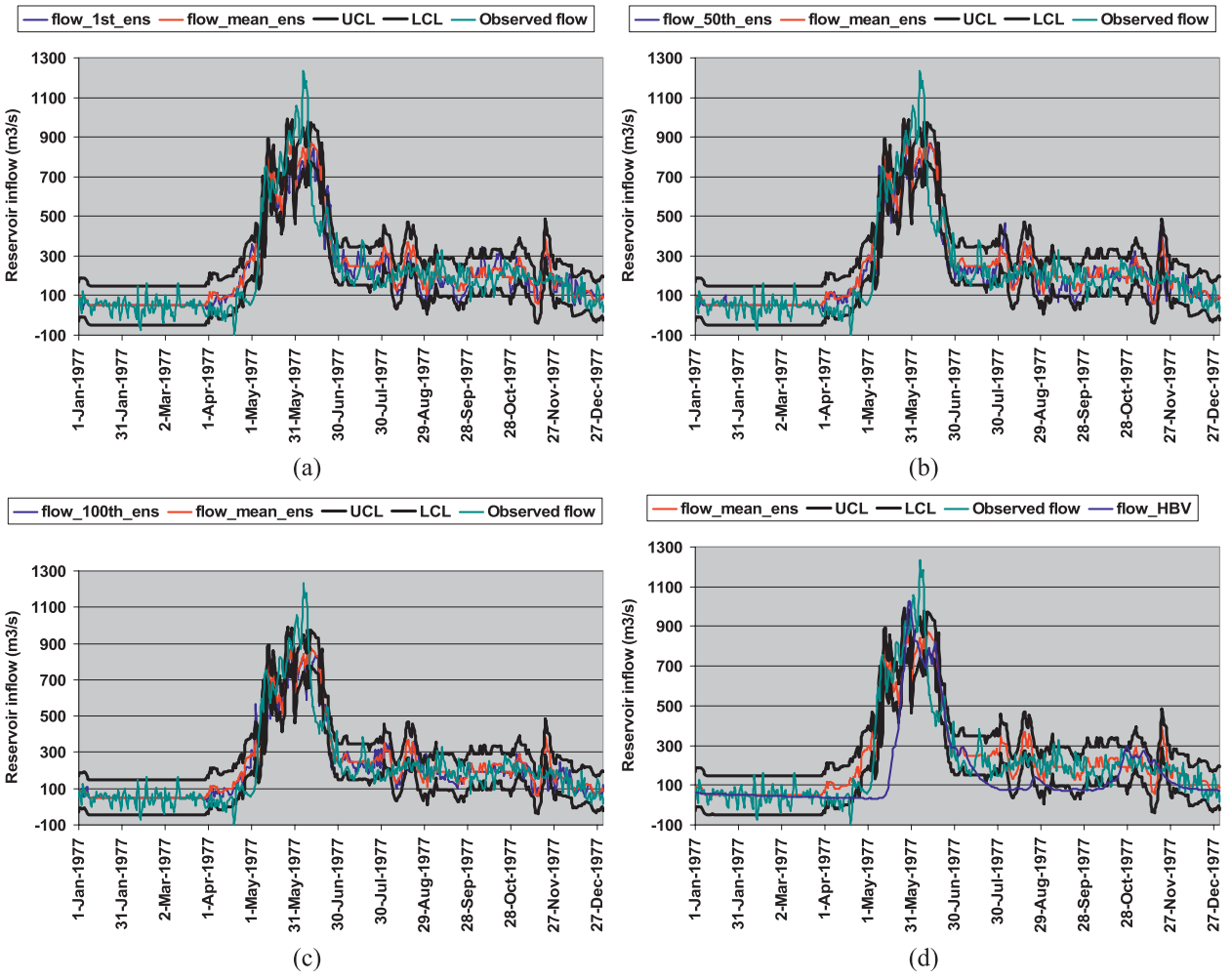

FIG. 4. Climate change impact on simulated reservoir inflow for the year 1997. Observed inflow, mean ensemble inflow, and its upper and lower confidence limits are plotted in (a) 1st ensemble inflow, (b) 50th ensemble inflow, (c) 100th ensemble inflow, and (d) HBV simulated inflow.

2100. The downscaled daily precipitation and temperature data were fed into the BNN model to simulate reservoir inflow. The following combination of inputs were used in the BNN model: (i) total daily precipitation of the last 12 days, starting from $t - 1$ to $t - 12$, is considered as 12 separate inputs; (ii) moving sum of the last 10 weeks' snow as another input; (iii) mean daily temperature at $t - 1$; (iv) moving average of the last 9 weeks' mean daily temperature; and (v) months (January–December) as logical inputs. Details of the downscaling experiments and the hydrological modeling with the BNN were described in separate studies, undertaken by Khan et al. (2006a,b) and Khan and Coulibaly (2006), respectively.

Predicted reservoir inflow with climate change impact for the years 1977 and 2043 is presented in Figs. 4 and 5, respectively. In those figures, the mean ensemble flow and its 95% confidence intervals were simulated with CGCM1 IS92a emission scenario. Observed reservoir inflow for the year 1977 is also plotted in Fig. 4. A comparison of basic statistics, such as mean and standard deviation for observed and simulated flows for the year 1977, is also presented in Table 4. Some of the statistics, especially the standard deviations, are quite different between the observed and simulated flows for several months but the 95% uncertainty bands of the simulated flow mostly include the observed flow, with some exception during spring peak flow periods around May. For further comparison, in Fig. 4a, the 1st ensemble inflow is presented, which is the flow corresponding to the 1st downscaled ensemble member of daily precipitation and temperature for the CGCM1 IS92a scenario. Figure 4a shows that both the observed and the 1st ensemble flows are largely within the confidence intervals of the

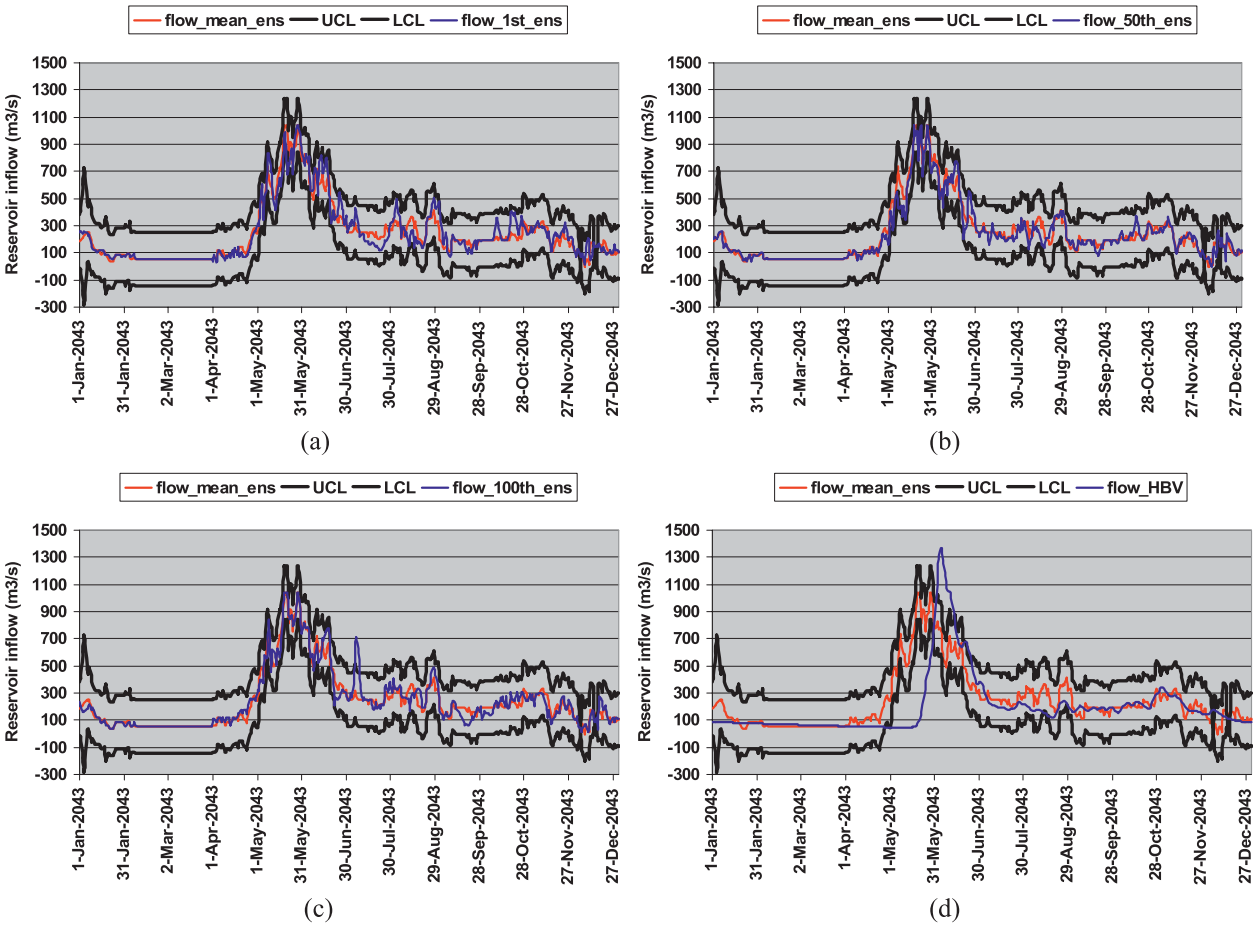

FIG. 5. As in Fig. 4, but for 2043.

mean ensemble flow. In Figs. 4b and 4c, the 50th and 100th ensemble flows are presented along with the mean ensemble flow and its confidence intervals. Both the 50th and 100th ensemble flows are also within the confidence intervals of the mean ensemble flow. In Fig. 4d, the HBV model–simulated reservoir inflows for the CGCM1 IS92a emission are presented. The HBV flows also lie mostly within the confidence interval of the BNN mean ensemble flow, except for the peak flows.

Predicted reservoir inflows for the future year, 2043, are presented in Fig. 5. The mean ensemble flow, in Figs. 5a–5d, and its 95% confidence intervals are simulated with CGCM1 IS92a emission scenario. In Figs. 5a, the 1st ensemble flows are simulated with CGCM1 IS92a emission scenario. In Figs. 5b and 5c, the 50th and 100th ensemble flows are simulated with CGCM2 SRES B2 scenario. In Fig. 5d, the HBV flow is simulated with CGCM1 IS92a emission scenario. In all Figs. 5a–5d, the 95% confidence intervals of the mean ensemble flow is able to mostly encompass all likely flows with a different version of CGCM and a different emission scenario, and also flows simulated with another hydrological model, HBV. Although the HBV flows are not all within the confidence bands, especially the spring peak flow in May, most of the hydrograph is within the confidence limits of the BNN predictions. The HBV model tends to overestimate the spring peak flow and a right sift of the hydrograph is also observed (Fig. 5d), which could be associated with the HBV model error. However, in general, the analysis confirms that the uncertainty bands generated using the mean ensemble member of downscaled meteorological variables with one version of CGCM along with one emission scenario are able to mostly encompass all likely flows associated with another version of CGCM, with another emission scenario, and with another hydrological model, both for the current and future periods.

8. Summary and conclusions

The objective of this study is to assess whether the Bayesian neural network (BNN) model could be used as an efficient hydrological modeling tool for climate

TABLE 4. As in Table 3, but for reservoir inflow for 1977.

	Observed		Simulated	
	Mean (m^3 s^{-1})	SD (m^3 s^{-1})	Mean (m^3 s^{-1})	SD (m^3 s^{-1})
Jan	53.065	31.775	57.929	11.263
Feb	44.404	49.785	50.855	0.087
Mar	43.671	40.833	51.443	3.586
Apr	41.817	47.774	135.360	69.948
May	623.771	258.151	575.264	158.500
Jun	639.933	302.069	647.831	188.058
Jul	208.190	58.897	254.283	40.881
Aug	209.200	31.573	237.724	73.469
Sep	204.093	53.720	180.550	45.152
Oct	185.090	49.936	209.675	55.141
Nov	188.520	25.000	200.417	70.370
Dec	101.865	55.655	116.424	38.890

change impact study on river flow and reservoir inflows with uncertainty estimates. The objective is proved by applying the BNN model to river flow and reservoir inflow simulations under climate change scenarios on two watersheds in northeastern Canada. Two GCliMs (CGCM1 and CGCM2) with two greenhouse gas emission scenarios (IPCC IS92a and SRES B2) and a statistical downscaling model (SDSM) are used in the investigation. It is found that the 95% confidence limits of the BNN-simulated mean ensemble flow (i.e., flow obtained by using the mean of 100 ensemble members of the downscaled daily precipitation, and daily maximum and minimum temperatures with CGCM1 IS92a emission scenario) is capable of mostly encompassing all other likely flows corresponding to randomly chosen downscaled meteorological ensemble members with CGCM1 IS92a and CGCM2 SRES B2 scenarios, and also most of the flows simulated by another hydrological model, HBV, with CGCM1 IS92a emission scenario. However, the model showed some deficiency in encompassing peak flows for both the river and reservoir inflow simulations—which warrants further improvement of the current BNN model. HBV-simulated peak flows were also not within the uncertainty bands of the BNN model predictions; a possible reason could be the HBV model error and/or the limitation of the current BNN model. However, in general, most findings suggest that the BNN-simulated mean ensemble flow and its confidence bands are capable of including most of the likely flows that can be obtained from various ensemble members of downscaled meteorological variables with different versions of CGCM and emission scenarios. This uncertainty management capacity of the BNN model is a promising aspect in climate change impact study on water resources. It can be a good alternative method in situations in which there is not enough resources to implement a multimodel ensembles approach. This will also eventually save time and effort in managing uncertainty by eliminating the scope of using multiple CGCMs and emission scenarios, and various hydrological models. This uncertainty management capacity of the BNN model can be further investigated using other GCliMs with various other emissions scenarios, and downscaling and hydrologic models. The efficiency of the BNN model for assessing the hydrologic impact of climate change with uncertainty estimates could be further improved by investigating complex MCMC approximation methods, such as the hybrid Monte Carlo method or the evolutionary Monte Carlo method.

Acknowledgments. This work is made possible through a grant from the Canadian Climate Change Action Fund, Environment Canada, and a grant from the Natural Sciences and Engineering Research Council of Canada. The authors thank the Aluminum Company of Canada (Alcan) for providing the experiment data. The IHMS-HBV has kindly been made available by the Swedish Meteorological and Hydrological Institute. The authors are grateful to three anonymous reviewers for their valuable comments and suggestions.

REFERENCES

Arnell, N., 1999: Uncertainty in climate change impact studies in the water sector. *Representing Uncertainty in Climate Change Scenarios and Impact Studies,* T. R. Carter, M. Hulme, and D. Viner, Eds., Climatic Research Unit ECLAT-2 Workshop Rep. 1, 85–88.

Bishop, C. M., 1995: *Neural Network for Pattern Recognition*. Clarendon Press, 482 pp.

Christensen, J. H., and Coauthors, 2007: Regional climate projections. *Climate Change 2007: The Physical Science Basis,* S. Solomon et al., Eds., Cambridge University Press, 847–940.

Coulibaly, P., 2008: Multi-model approach to hydrologic impact of climate change. *From Headwaters to the Ocean: Hydrological Changes and Watershed Management,* M. Taniguchi et al., Eds., CRC Press, 249–256.

——, F. Anctil, and B. Bobée, 2000: Daily reservoir inflow forecasting using artificial neural networks with stopped training approach. *J. Hydrol.,* **230,** 244–257.

——, B. Bobée, and F. Anctil, 2001a: Improving extreme hydrologic events forecasting using a new criterion for artificial neural network selection. *Hydrol. Processes,* **15,** 1533–1536.

——, F. Anctil, and B. Bobée, 2001b: Multivariate reservoir inflow forecasting using temporal neural networks. *J. Hydrol. Eng.,* **6,** 367–376.

——, Y. B. Dibike, and F. Anctil, 2005: Downscaling precipitation and temperature with temporal neural networks. *J. Hydrometeor.,* **6,** 483–496.

Dibike, Y. B., and P. Coulibaly, 2005: Hydrologic impact of climate change in the Saguenay watershed: Comparison of downscaling methods and hydrologic models. *J. Hydrol.,* **307,** 145–163.

——, and ——, 2007: Validation of hydrological models for climate scenario simulation: The case of Saguenay watershed in Quebec. *Hydrol. Processes,* **21,** 3123–3135.

Flato, G. M., and W. D. Hibler, 1992: Modeling pack ice as a cavitating fluid. *J. Phys. Oceanogr.,* **22,** 626–651.

——, and G. J. Boer, 2001: Warming asymmetry in climate change simulations. *Geophys. Res. Lett.,* **28,** 195–198.

——, ——, W. G. Lee, N. A. McFarlane, D. Ramsden, M. C. Reader, and A. J. Weaver, 2000: The Canadian Centre for Climate Modelling and Analysis global coupled model and its climate. *Climate Dyn.,* **16,** 451–467.

Fowler, H. J., S. Blenkinsop, and C. Tebaldi, 2007: Linking climate change modeling to impacts studies: Recent advances in downscaling techniques for hydrological modeling. *Int. J. Climatol.,* **27,** 1543–1545.

Frederic, K. D., and D. C. Major, 1997: Climate change and water resources. *Climatic Change,* **37,** 7–23.

Gent, P. R., and J. C. McWilliams, 1990: Isopycnal mixing in ocean circulation models. *J. Phys. Oceanogr.,* **20,** 150–155.

Hulme, M., and T. R. Carter, 1999: Representing uncertainty in climate change scenarios and impact studies. *Representing Uncertainty in Climate Change Scenarios and Impact Studies,* T. R. Carter, M. Hulme, and D. Viner, Eds., Climatic Research Unit ECLAT-2 Workshop Rep. 1, 11–37.

Jana, R. B., B. P. Mohanty, and E. P. Springer, 2008: Multiscale Bayesian neural networks for soil water content estimation. *Water Resour. Res.,* **44,** W08408, doi:10.1029/2008WR006879.

Khan, M. S., and P. Coulibaly, 2006: Bayesian neural network for rainfall-runoff modeling. *Water Resour. Res.,* **42,** W07409, doi:10.1029/2005WR003971.

——, ——, and Y. Dibike, 2006a: Uncertainty analysis of statistical downscaling methods. *J. Hydrol.,* **319,** 357–382.

——, ——, and ——, 2006b: Uncertainty analysis of statistical downscaling methods using Canadian Global Climate Model predictors. *Hydrol. Processes,* **20,** 3085–3104, doi:10.1002/hyp.6084.

Kingston, G. B., M. F. Lambert, and H. R. Maier, 2005: Bayesian training of artificial neural networks used for water resources modeling. *Water Resour. Res.,* **41,** W12409, doi:10.1029/2005WR004152.

Lampinen, J., and A. Vehtari, 2001: Bayesian approach for neural networks – Review and case studies. *Neural Networks,* **14,** 257–274.

MacKay, D. J. C., 1992a: A practical Bayesian framework for backpropagation networks. *Neural Comput.,* **4,** 448–472.

——, 1992b: Bayesian interpolation. *Neural Comput.,* **4,** 415–447.

McCarthy, J. J., O. F. Canziani, N. A. Leary, D. J. Dokken, and K. S. White, Eds., 2001: *Climate Change 2001: Impacts, Adaptation, and Vulnerability*. Cambridge University Press, 1032 pp.

McFarlane, N. A., G. J. Boer, J.-P. Blanchet, and M. Lazare, 1992: The Canadian Climate Centre second-generation general circulation model and its equilibrium climate. *J. Climate,* **5,** 1013–1044.

Nabney, I. T., 2004: *NETLAB: Algorithms for Pattern Recognition*. Springer-Verlag, 420 pp.

Neal, R. M., 1992: Bayesian training of backpropagation networks by the hybrid Monte Carlo method. Department of Computer Science, University of Toronto, Technical Rep. CRG-TR-92-1, 21 pp.

——, 1993: Bayesian learning via stochastic dynamics. *Advances in Neural Information Processing Systems 5,* C. L. Giles et al., Eds., Morgan Kaufmann, 475–482.

——, 1996: *Bayesian Learning for Neural Networks*. Lecture Notes in Statistics, Vol. 118, Springer-Verlag, 183 pp.

Prudhomme, C., D. Jakob, and C. Svensson, 2003: Uncertainty and climate change impact on the flood regime of small UK catchments. *J. Hydrol.,* **277,** 1–23.

Semenov, M. A., and E. M. Barrow, 1997: Use of a stochastic weather generator in the development of climate change scenarios. *Climatic Change,* **35,** 397–414.

Shamseldin, A. Y., 1997: Application of a neural network technique to rainfall-runoff modeling. *J. Hydrol.,* **199,** 272–294.

SMHI, 1996: Integrated hydrological modeling system (IHMS) manual, version 4.5. Swedish Meteorological and Hydrological Institute.

Walker, A. M., 1969: On the asymptotic behaviour of posterior distributions. *J. Roy. Stat. Soc.,* **B31,** 80–88.

Wilby, R. L., and I. Harris, 2006: A framework for assessing uncertainties in climate change impacts: Low-flow scenarios for the River Thames, UK. *Water Resour. Res.,* **42,** W02419, doi:10.1029/2005WR004065.

——, C. W. Dawson, and E. M. Barrow, 2002: SDSM – A decision support tool for the assessment of regional climate change impacts. *Environ. Modell. Software,* **17,** 147–159.